

Preparation and molten salt-assisted KOH activation of porous carbon nanofibers for use as supercapacitor electrodes

Chang Ma¹ · Ranran Wang¹ · Zhenyu Xie¹ · Haixia Zhang¹ · Zhengyi Li¹ · Jingli Shi¹

Published online: 9 February 2017
© Springer Science+Business Media New York 2017

Abstract Carbon nanofiber paper was prepared by electrospinning from thermosetting phenolic resin, followed by activation via KOH-containing molten salt at high temperature. By adding a small dosage of KOH in the molten salt the porous volume and specific surface area could be greatly improved. The obtained porous carbon nanofibers had a specific surface area of $1007 \text{ m}^2 \text{ g}^{-1}$, total pore volume of $0.363 \text{ cm}^3 \text{ g}^{-1}$, micropore volume of $0.247 \text{ cm}^3 \text{ g}^{-1}$. The electrochemical measurements in 6 M KOH aqueous solution showed that the porous carbon nanofibers possessed high specific capacitance and considerable rate performance. The maximal specific capacitance of 288 F g^{-1} was achieved at 0.2 A g^{-1} and the specific capacitance could still remain 204 F g^{-1} at 20 A g^{-1} with the retention of 71%. In the molten salt system, the reaction between activating agent and carbon could be more efficient, hence, such molten salt-assisted activation method was considered as a general activation method for the high-specific-surface-area carbons.

Keywords Porous carbon nanofiber · Molten salt-assisted · KOH activation · Supercapacitor

1 Introduction

Electrochemical capacitors (known as ultracapacitors or supercapacitors) have recently attracted much attention because of their merits of high instant power density, quick charge and discharge processes, and excellent long-term stability [1–3]. Based on the energy storage mechanism of electrochemical capacitors, it can be classified into two main types as electrical double-layer capacitors and pseudocapacitors [4]. As is known, the capacitance performance of electrical double-layer capacitors greatly depends on electrodes. Being compared with other electrode materials, porous carbons are considered promising due to lower cost, better electronic conductivity, high surface area and high chemical stability [5–8]. Normally, porous carbons for supercapacitors are in form of powder. Therefore, a complex process is needed to prepare electrodes. Binder is necessary in the process of preparing electrodes and it would increase the resistance of electrodes and greatly lower the performance of supercapacitors [9].

Electrospun carbon nanofiber paper (ECNP) is widely used as electric double-layer capacitors electrode material, and it has attracted wide attention of researchers due to low cost, simple process and good flexibility [10–14]. It can be directly used as electrode material for electric double-layer capacitors without the usage of binders and the tedious preparation process of electrodes. In addition, three dimensional network structure endows it good electrical conductivity, which is conducive to ion conduction [15–17]. Most of the porous carbon nanofibers (PCNFs) for electrode materials are prepared by electrospun precursor solutions of incorporating porogen [18, 19] or by physical or chemical activation method [20, 21]. However, the above methods usually involve expensive templates/raw materials for template method or lead to relatively low

✉ Chang Ma
fdoy_lt54@163.com

✉ Jingli Shi
shijingli1963@163.com

¹ State Key Laboratory of Separation Membranes and Membrane Processes, School of Materials Science and Engineering, Tianjin Polytechnic University, Tianjin 300387, China

specific surface area for physical activation. Chemical activation, e.g. KOH-activation, is considered to be a relatively effective approach to prepare high-performanced PCNFs [22–24]. In addition, KOH-activation, also can improve surface oxygen [22], which helps to improve the capacitive performance of PCNFs-based supercapacitor. In our previous work, KOH-incorporating activation [22] and KOH-coating activation [25] have been tried. It is found that for KOH-incorporating activation, KOH amount was limited by spinnability and the increment of surface area was not remarkable. For KOH-coating activation, besides a large KOH consumption, there is a contradiction between the surface area and the structural stability of the fiber network because of the uncontrollable and intense interface reaction. Therefore, it is still of a high practical significance to acquire flexible ECNP with high surface area and good structural stability.

In recent years, low-melting-point molten salts, have been employed to assist synthesis of porous materials [26–29]. Molten salt as a reaction medium could effectively slows reaction rate and greatly improves the efficiency of activation agent. It helps to achieve a high surface area at the expense of less activation agent and restrain structural collapse. In this study, KOH-containing molten salt was used to treat phenolic-based nanofiber paper (PNP) at high temperature. The as-prepared carbon nanofiber paper kept intact and showed a considerable specific surface area and porosity. The electrochemical measurements in 6 M KOH aqueous solution showed that the obtained carbon nanofibers could deliver a maximal specific capacitance of 288 F g⁻¹ at 0.2 A g⁻¹ and 204 F g⁻¹ at 20 A g⁻¹ with the retention of 71%, showing an excellent capacitive performance.

2 Experimental

2.1 Preparation of phenolic-based activated carbon nanofiber paper

The synthesis of PNP was conducted according to the reported procedures [30], which including the synthesis of the spinning solution, electrospinning and curing. Phenol formaldehyde resin solution was obtained with a formaldehyde/phenol mole ratio of 1.45 under the base catalyst, then it is diluted to 18 wt% as spinning solution. After electrospinning process, the as-electrospun fibers were cured under 150 °C in air for 1 h. The as-prepared phenolic-based nanofibers paper was named as PNP.

In the next process, KOH was mixed with mixed salt of sodium fluoride (NaF) and sodium chloride (NaCl) at a weight ratio of 1(KOH):1(NaF):19(NaCl). In the mixed salt, KOH was active salt, which would turn to active ions at high temperature. The mixed salt NaF and NaCl was

inert salt, which was used as solvent and diluent. The composition and proportion of the mixed salt was determined according to three principles: (1) the melting point should lower than carbonization temperature; (2) the molten salt has a low saturation vapor pressure; (3) the salt should be cheap and available. The KOH-containing mixed salt was laid on a cut PNP with the KOH/PNP mass ratio of 5:1. The mixtures were pre-treated at 120 °C for 2 h in air to remove moisture followed by thermal treatment at 800 °C in nitrogen for 1 h with a heating rate of 3 °C min⁻¹. Afterward, the obtained complex was treated with excess diluted hydrochloric acid and repeatedly flushed with distilled water until the filtrate reached neutral pH, to acquire carbon nanofiber paper. The carbon nanofibers treated by KOH-containing molten salt was denoted as KTCN. Sample treated with KOH-free molten salt was denoted as MTCN and that without molten-salt treatment was denoted as CN.

2.2 Materials characterizations

The morphology and structure of samples were examined by field-emission scanning electron microscopy (FESEM, HitachiS-4800) and transmission electron microscopy (TEM, JEOL, JEM-2100). The porous texture was characterized by N₂ adsorption/desorption at 77 K using an automatic adsorption system (Tristar 3020, Micromeritics). All samples were degassed at 300 °C for 10 h before the measurements. The specific surface areas were measured using the Brunauer Emmette Teller (BET) equation. Pore volume was calculated from the adsorbed amount at a relative pressure P/P₀=0.994. X-ray diffraction (XRD) analyses were carried out using a Rigaku D/max-ga diffractometer with graphite monochromatized using CuK_α radiation (λ=0.15406 nm) at room temperature. X-ray photoelectron spectroscopy (XPS) was measured by a X-ray photoelectron spectrometer (ESCALAB 250) to analyze the surface characteristics of the samples.

2.3 Electrochemical measurement

The electrochemical performance of all samples was examined using a three-electrode system with 6 M KOH aqueous solution as electrolyte. Working electrodes were fabricated by pressing carbon nanofiber film between two pieces of circular nickel foams. In these tests, all samples were directly used as the working electrode without any polymer binder and conductive graphite. A Pt plate and a Hg/HgO electrode were used as counter electrode and reference electrode, respectively. Before testing, the working electrodes were immersed in 6 M KOH solution for 24 h. Cyclic voltammetry (CV) was determined at a scan rate from 5 to 100 mV s⁻¹, and the galvanostatic charge and discharge was measured at current density from 0.2 to

20 A g⁻¹. All the CV and galvanostatic charge/discharge measurements were conducted in the potential range from -0.9 to 0 V (vs. Hg/HgO). For electrochemical impedance spectroscopy (EIS), the frequency range was from 0.01 Hz to 100 kHz. All the electrochemical tests were performed using CHI 660 C instrument (Shanghai Chenhua Apparatus Co. Ltd.) at the room temperature.

3 Results and discussion

3.1 Morphology and textural properties

A significant feature of ECNPs, also a prominent advantage, is the self-sustaining nature, due to which ECNPs could be directly cut into electrodes avoiding complex preparation process of electrodes. Figure 1a show the optical images of PNP and KTCN, both of which have a smooth surface. Figure 1b–d shows the SEM images of CN, MTCN and KTCN, respectively. All the samples have complete fiber morphology and the fibers stack randomly to form a network structure. The morphology of the fiber is intact even after treatment by molten salt method. For KOH-coating activation, with the increase of KOH concentration, the fiber morphology was obviously distorted and surface erosion of fibers is serious [25]. For molten salt-assisted KOH activation, the phenomenon of distortion and surface erosion can not be found. It implies a more modest interface reaction. The molten salt played an important role in slowing the reaction rate and increasing reaction homogeneity.

Fig. 1 Photographs of **a** PNP and KTCN, and SEM micrographs of **b** CN, **c** MTCN, **d** KTCN

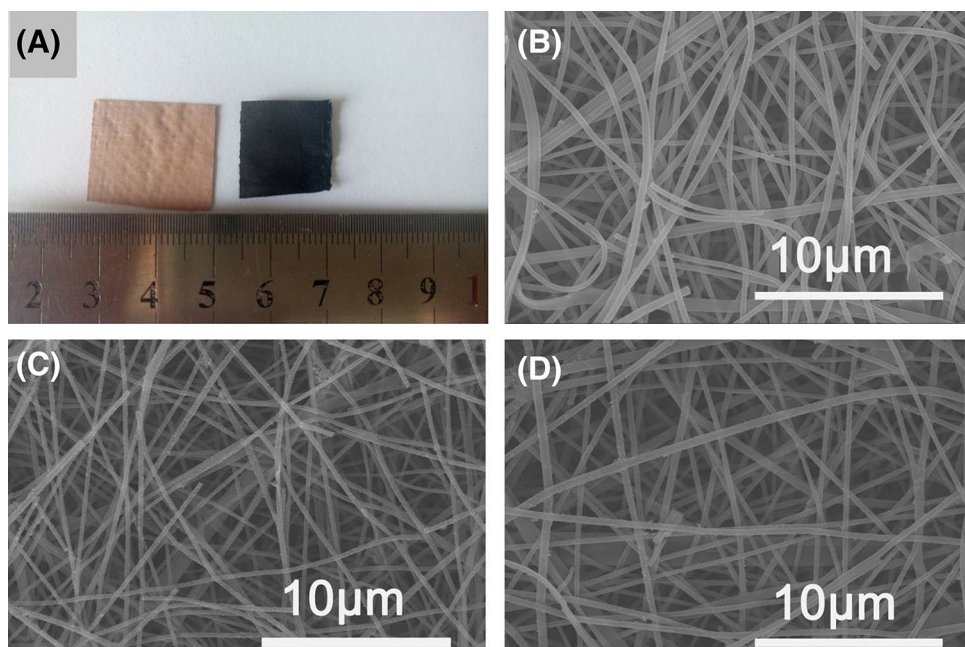


Figure 2 shows TEM images of KTCN under different magnifications. As is seen from Fig. 2a, the surface

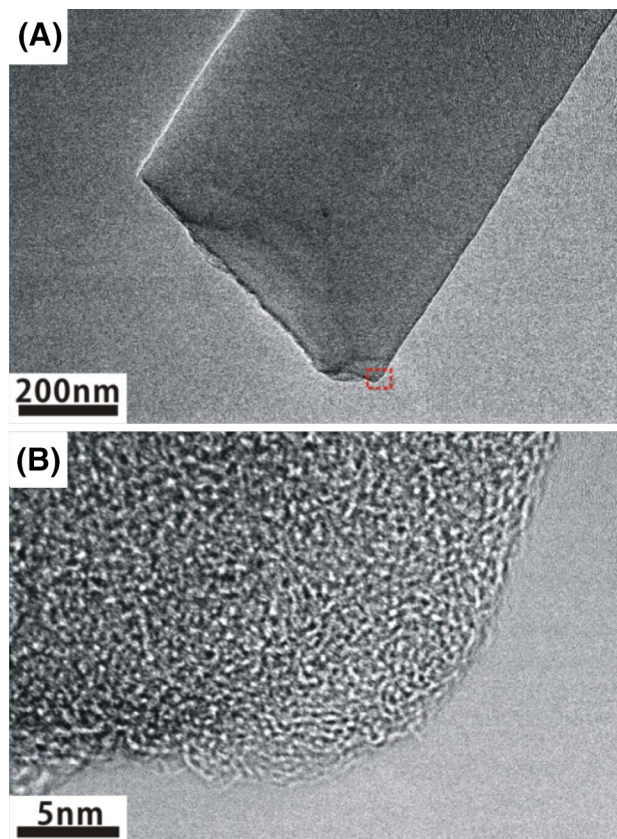


Fig. 2 TEM images of carbon nanofibers under different magnifications

of carbon nanofiber is relatively smooth, and no secondary phase aggregates are observed. Figure 2b shows the microstructure of the fiber at high magnification. Abundant micropores can be observed interconnected to each other. There is no crystalline phase, suggesting a typical amorphous characteristic.

In order to further examine the structure, phase composition and degree of graphite of all samples, XRD patterns of samples were recorded, as shown in Fig. 3. For all samples, the observation of broad (002) peak and (100) peak appeared at around 21° and 43° is indicative of amorphous structure of carbon [31, 32]. The intensity of diffraction peak of KTCN becomes weaker, which indicates that the KOH activation increases the disorder degree of the sample structure, and causes the destruction of the graphite layer [33].

Figure 4a shows the nitrogen adsorption/desorption isotherms of all samples. It can be seen that the adsorption/desorption isotherms of MTCN and CN are almost coincident, indicating that the adsorption capacity of the two is almost equal. The adsorption isotherms of KTCN express a type I behavior for the micropore adsorption, with an obvious hysteresis loop, indicating the existence of the mesopores. The activation mechanism of KOH has been investigated widely for many years. The total reaction between carbon and KOH is: $6\text{KOH} + \text{C} = 2\text{K} + 3\text{H}_2 + 2\text{K}_2\text{CO}_3$ [34]. Practically speaking, there are three aspects that contribute to the formation of pores: first, the most chaotic and the most active carbon removal; second, carbon matrix in the removal of large molecular weight; third, the reaction product metal potassium through the insertion of graphite layer to make holes [35]. For traditional process, KOH contacts with carbon in form of particle or coating. In condition of high temperature, KOH melts and covers on the surface of

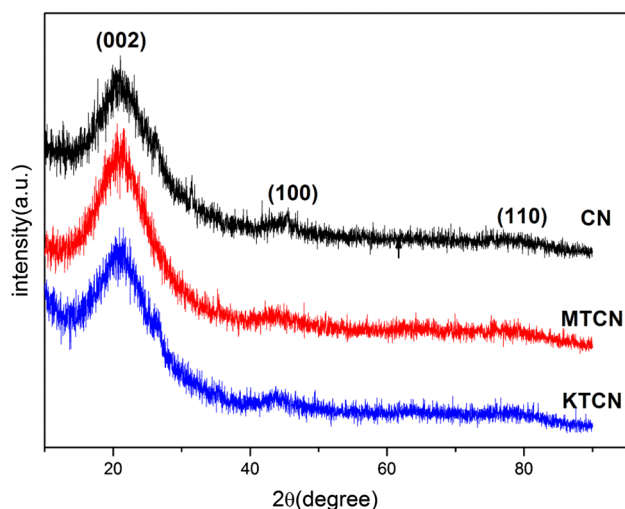


Fig. 3 XRD pattern of all samples

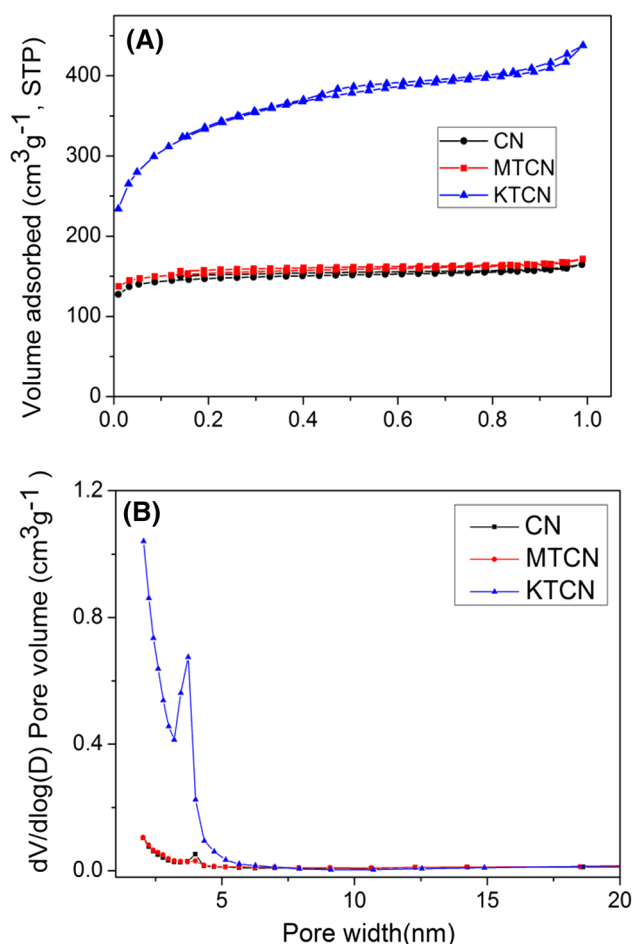


Fig. 4 N_2 adsorption–desorption isotherms (a) and calculated pore size distribution (b) of all samples

carbon. The reaction occurs from the surface to interior. To cover all the surface of carbon completely, KOH consumption should be enough. Considering the nonuniformity derived from gravity or aggregate, more KOH is better. However, in the molten salt, KOH is dispersed in the form of ions, as shown in Fig. 5. The contact of KOH and carbon is completely uniform, and complete cover and uniform reaction is easy to achieve. In addition, reaction product, including K and K_2O , would evaporate greatly because of a large solid–gas interface. For the molten salt-assisted activation, the liquid melt salt medium played an important role in restraining the escape of the activation agent, including KOH, K, K_2O and K_2CO_3 . Figure 4b shows the pore size distributions of all samples. Usually, KOH-activation introduces micropores principally [22]. Similarly, the molten salt-assisted activation principally produce micropores. However, it is worth pointing out that a small quantity of mesopores were generated. It suggests that both high activation degree and intact appearance can be achieved using molten salt-assisted activation method.

Fig. 5 Schematic depiction of molten salt-assisted KOH activation

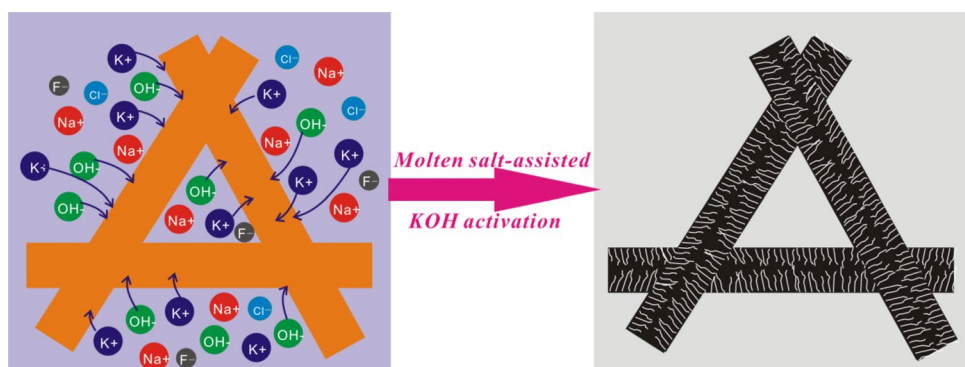


Table 1 Pore structure parameters of all samples

Sample	S_{BET} ($m^2 g^{-1}$)	S_{micro} ($m^2 g^{-1}$)	V_{total} ($cm^3 g^{-1}$)	V_{micro} ($cm^3 g^{-1}$)	V_{micro}/V_{total} (%)
CN	449	382	0.198	0.191	96
MTCN	468	402	0.208	0.193	93
KTCN	1007	389	0.364	0.247	68

The detailed porous structure parameters are displayed in Table 1. It can be seen that the parameters of CN and MTCN are almost the same. It demonstrates that the molten salt itself has no effect on the porosity and specific surface area. The much increased specific surface area and higher porosity of KTCN prove that KOH, specific speaking KOH in the molten salt, plays a positive role in producing pores. KTCN possesses a specific surface area of $1007 m^2 g^{-1}$, total pore volume of $0.364 cm^3 g^{-1}$, both much higher than that of MCNF-K-20% using one-step activation method [22]. Moreover, after molten salt-assisted KOH treatment, the KTCN has a enhanced mesoporosity of 32%, higher than that of CN (4%) and MTCN (7%). It has been largely reported that mesopores can reduce the transmission resistance of electrolyte ions, provide a low-resistance channel for ions, then improve the capacitive behavior of the carbon material, especially at high current loading [36].

3.2 The surface chemistry of CNFs

In order to figure out the chemical nature of the functional groups, all samples were investigated using XPS measurement. The XPS spectra of all samples are shown in Fig. 6. It can be seen that all the samples have two obvious peaks, respectively, on behalf of C and O. No K peak is observed, demonstrating the K species has been removed completely. The fitting results of O1s peaks for all samples are showed in Fig. 7. The elemental composition of all samples and the relative content of different oxygen species are showed in Table 2. As is seen, the types of oxygen functional groups

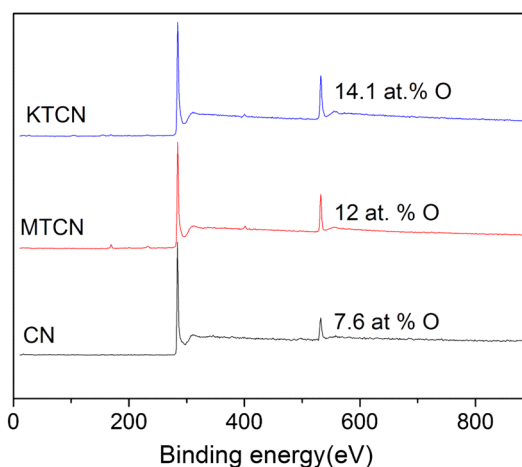


Fig. 6 XPS survey spectra of all samples

have not changed after activation treatment. The O1s spectra is deconvoluted into three peaks centered at around 531.8, 532.8 and 535.2 eV, which can be ascribed to the C=O groups (OI), C–OH groups (OII) and chemisorbed oxygen (carboxylic groups) and/or water (OIII), respectively [37]. It can be found clearly that the high temperature molten salt make a positive influence on the oxygen content, increasing the oxygen content from 7.6 to 12%. Being compared with opening gas environment, molten salt liquid environment is more beneficial for retaining oxygen, which escapes from the fibers during the thermal pyrolysis in the form of CO, CO₂, H₂O, etc. Introduction of KOH in molten salt further adds oxygen because KOH itself contains oxygen. It can be seen that the molten salt treatment mainly bring about C–OH groups (OII), while the introduction KOH further add the chemisorbed oxygen (carboxylic groups) and/or water.

3.3 Electrochemical performance

The electrochemical property of the obtained porous flexible carbon fiber paper were investigated by three-electrode

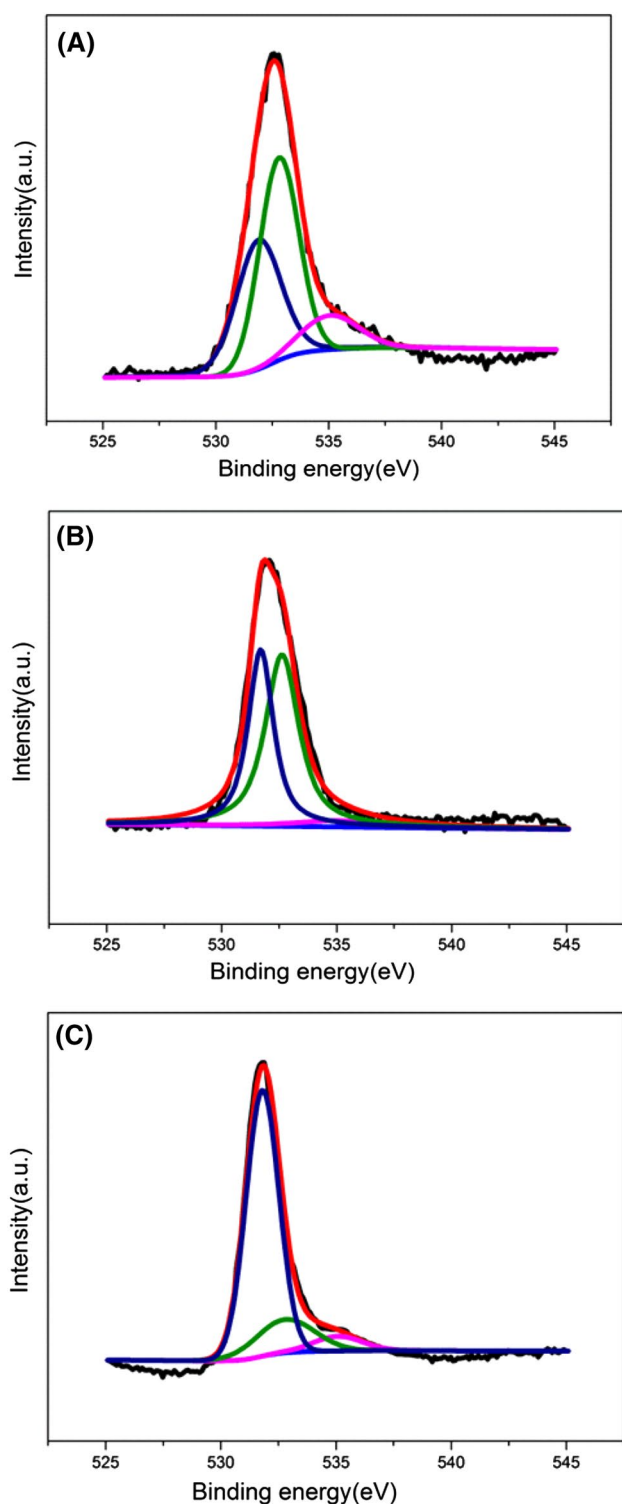


Fig. 7 XPS spectra of O1s for all samples **a** KTCN; **b** MTCN; **c** CN

system. Figure 8a shows the CV curves of all samples at scan rate of 5 mV s^{-1} within a potential window from -0.9 to 0 V (vs. Hg/HgO). For ideal double-electric layer capacitor, the CVs are shaped like a rectangular. The CV

profiles in our case present a huge hump at low potential, which indicates that the presence of the faradaic reaction related to the surface oxygen-containing functional groups. KTCN has the largest surrounding area, which shows that the specific capacitance is much enhanced, which is due to its increased surface area. Figure 8b shows the CV curves of all samples at scan rate of 100 mV s^{-1} . Rectangular shape of CV curves are remained even at a high scan rate of 100 mV s^{-1} for KTCN, which indicates that the movement of charge, including electron in electrode and ions in the pores, is high-speed even at high scan rate in spite of a high porosity and specific surface area.

Figure 9a, b shows the galvanostatic charge/discharge curves for various samples at current density of 0.2 and 10 A g^{-1} . For ideal double-electric layer capacitor, the charge/discharge curves are shaped like a straight line. The galvanostatic charge/discharge curves in our case are not strict linear, which indicates that the redox reaction of the oxygen-containing groups with electrochemical activity [37]. KTCN has a much longer discharge time, shown its superior capacitance performance. It is in agreement with the results of CVs for the three electrode. Figure 9c shows the galvanostatic charge/discharge curves of KTCN electrode at different current densities. At big current loading, the charge/discharge curves turn to linear and symmetry, suggesting a good reversibility. The capacitance was calculated on the basis of the galvanostatic charge and discharge curve according to the following equation.

$$C = (I \cdot \Delta t) / (m \cdot \Delta V)$$

where I is the constant discharging current (A), Δt is the discharge time (s), m is the mass of active materials in single electrode and ΔV is the potential difference (0.9 V in the study). Figure 9d shows the trend of specific capacitance with current density in 6 M KOH solution in three-electrode cell. At a current density of 0.2 A g^{-1} , the specific capacitance was calculated to be 200 , 215 and 288 F g^{-1} for CN, MTCN and KTCN, respectively. The results follows the law that the bigger the specific surface area, the higher the specific capacitance. The specific capacitance decreases gradually with the increasing of current density, which is common for carbon based electrodes. It is because that the surface availability of pores becomes lower and lower with the increasing of current loading. However, even at large current density of 20 A g^{-1} , KTCN still maintain a large specific capacitance of 204 F g^{-1} , which is in the highest level for ENCPs [10, 21, 22, 25, 38–44].

Figure 10 shows the electrochemical impedance spectroscopy measured in the range from 0.01 to 100 kHz in the three-electrode cell. All of the impedance diagrams showing the characteristics of the typical porous carbon electrode, consists of the high-frequency semicircle, frequency of 45° diagonal and low frequency region near vertical on

Table 2 Chemical composition of samples

Sample	XPS (at.%)					
	C	O	C/O	OI	OII	OIII
KTCN	85.9	14.1	6.1	5.6	6.9	1.6
MTCN	88	12	7.3	5.0	6.4	0.6
CN	92.4	7.6	12.2	5.8	1.3	0.5

Fig. 8 **a** CV curves for all samples at scan rate of 5 mV s⁻¹. **b** CV curves for all samples at scan rate of 100 mV s⁻¹

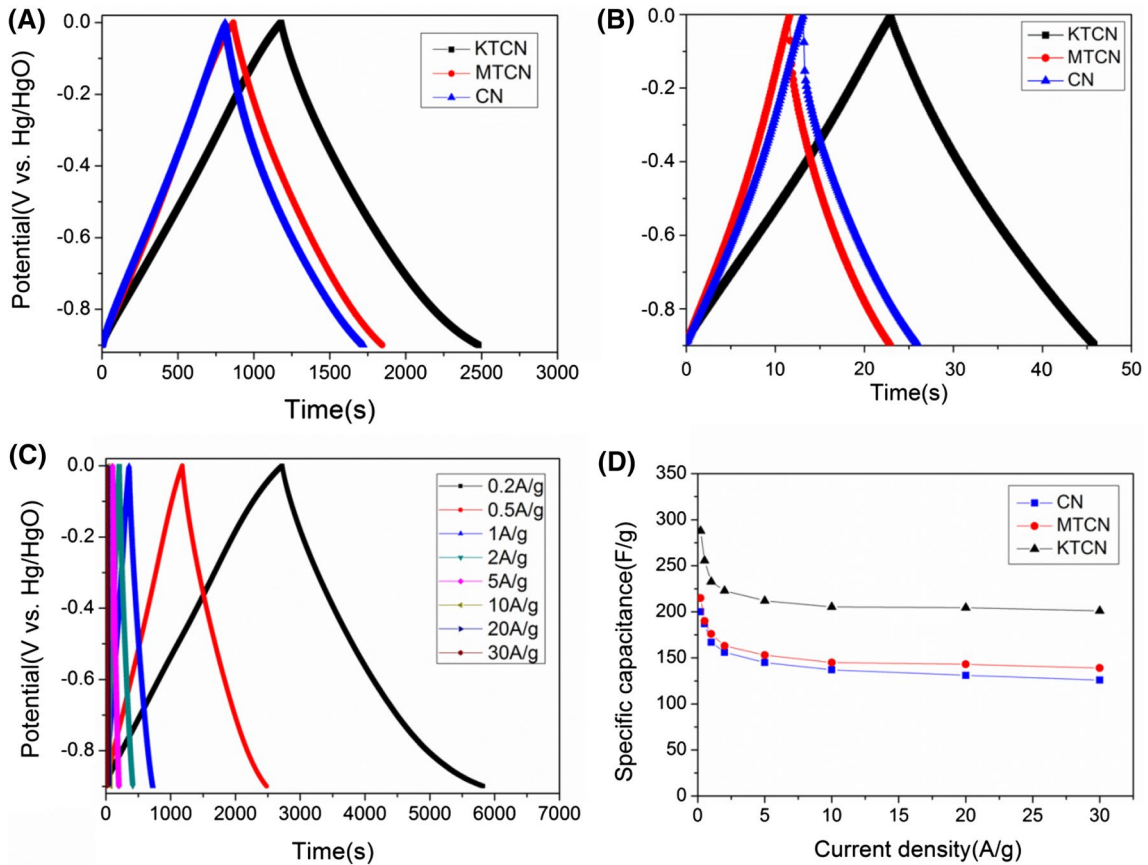
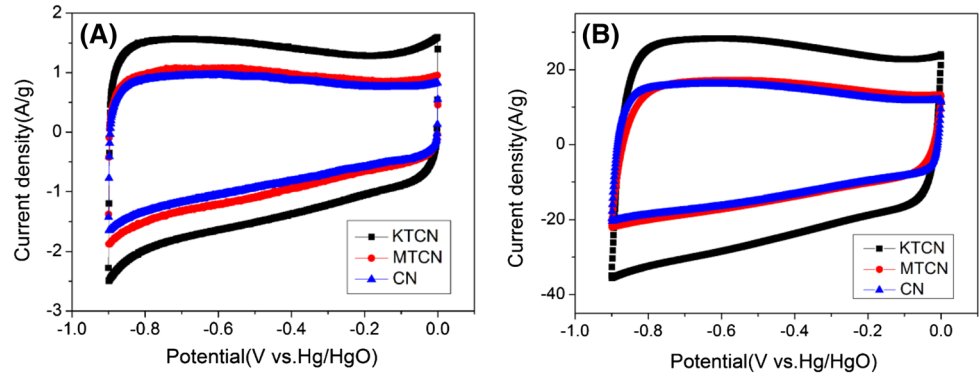


Fig. 9 **a** Charge and discharge curves of all samples at 0.2 A g⁻¹. **b** Charge and discharge curves of all samples at 10 A g⁻¹. **c** Charge and discharge curves of KTCN at various current density. **d** Specific capacitances of all samples at different current densities

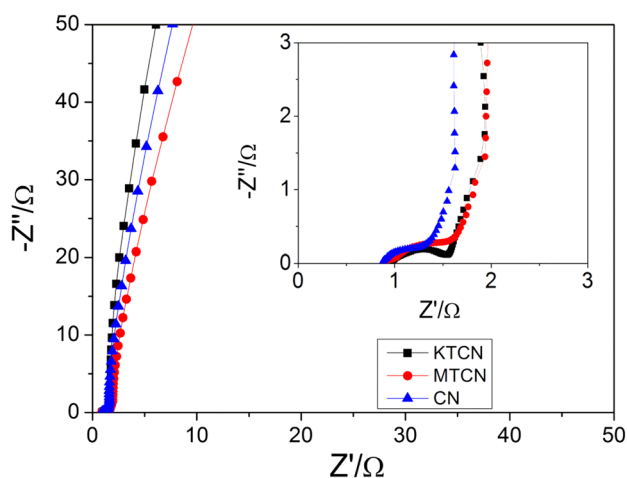


Fig. 10 Nyquist plots of electrodes, and the *inset* is the amplification of high frequency region

the X axis linear. In high frequency region, the starting point can represent the resistance of electrolyte. Because all the samples are used in the same assembly process as well as the same electrolyte, so semicircle starting point of all the samples are consistent. Considering the same electrolyte resistance and contact resistance, the semicircular arc at high frequencies represents the resistance of the electrode. KTCN has the largest resistance. It should be mainly attributed to higher porosity of KTCN. Generally, the higher the porosity, the poorer the conductivity. At low frequency region, three electrodes show straight line almost perpendicular to the X axis. It shows that the ion can be very fast diffusion adsorption at low frequency. It is believed that the nanometered pore depth played a positive role for it.

4 Conclusions

In summary, a porous carbon nanofiber with high specific surface area was successfully prepared from thermosetting phenolic resin via a facile molten salt-assisted KOH activation method. Compared to the traditional activation method, much less KOH dosage can achieve a fairly good activation effect and high porosity and specific surface area. The as-prepared carbon nanofibers had rich micropores and mesopores with a high specific surface area of $1007 \text{ m}^2 \text{ g}^{-1}$. The as-prepared carbon nanofibers can be directly used as electrode for supercapacitors free of binder. High specific capacitances (288 F g^{-1} at 0.2 A g^{-1}) and good capacitance retention rate (71%) were achieved. The molten salt-assisted activation method would be an universal and promising method to activated carbons. And such high specific

surface-aread carbon nanofibers will provide a promising candidate for the applications in supercapacitors.

Acknowledgements The authors would like to thank financial support from National Nature Science Foundation of China (Grant No. 51502201) and Natural Science Foundation of Tianjin Province (Grant No. 16JQJNC06300).

References

1. X. Huang, Z. Zeng, Z. Fan, J. Liu, H. Zhang, *Adv. Mater.* **24**, 5979 (2012)
2. L.L. Zhang, X.S. Zhao, *Chem. Soc. Rev.* **38**, 2520 (2009)
3. X. He, N. Zhang, X. Shao, M. Wu, M. Yu, J. Qiu, *Chem. Eng. J.* **297**, 121 (2016)
4. P. Simon, Y. Gogotsi, *Nat. Mater.* **7**, 845 (2008)
5. Y. Zhai, Y. Dou, D. Zhao, P.F. Fulvio, R.T. Mayes, S. Dai, *Adv. Mater.* **23**, 4828 (2011)
6. D.A.G. Hegde, *RSC Adv.* **5**, 88339 (2015)
7. X. Fan, C. Yu, J. Yang, Z. Ling, C. Hu, M. Zhang, J. Qiu, *Adv. Energy Mater.* **5**, 1401761 (2015)
8. X. Fan, C. Yu, Z. Ling, J. Yang, J. Qiu, *ACS Appl. Mater. Interfaces* **5**, 2104 (2013)
9. V. Presser, L. Zhang, J.J. Niu, J. McDonough, C. Perez, H. Fong, Y. Gogotsi, *Adv. Energy Mater.* **1**, 423 (2011)
10. C. Kim, B.T.N. Ngoc, K.S. Yang, M. Kojima, Y.A. Kim, Y.J. Kim, M. Endo, S.C. Yang, *Adv. Mater.* **19**, 2341 (2007)
11. Y. Gao, V. Presser, L. Zhang, J.J. Niu, J.K. McDonough, C.R. Pérez, H. Lin, H. Fong, Y. Gogotsi, *J. Power Sources* **201**, 368 (2012)
12. Y. Ren, J. Dai, B. Pang, X. Liu, J. Yu, *Electrochim. Acta* **176**, 402 (2015)
13. B.-H. Kim, K.S. Yang, H.-G. Woo, *Electrochem. Commun.* **13**, 1042 (2011)
14. Z.-L. Wang, D. Xu, J.-J. Xu, L.-L. Zhang, X.-B. Zhang, *Adv. Funct. Mater.* **22**, 3699 (2012)
15. J. Chmiola, C. Largeot, P.-L. Taberna, P. Simon, Y. Gogotsi, *Science* **328**, 480 (2010)
16. L. Zhang, Y. Jiang, L. Wang, C. Zhang, S. Liu, *Electrochim. Acta* **196**, 189 (2016)
17. Z. Wu, X.-L. Huang, Z.-L. Wang, J.-J. Xu, H.-G. Wang, X.-B. Zhang, *Sci. Rep.* **4**, 3669 (2014)
18. L. Zeng, W. Li, J. Cheng, J. Wang, X. Liu, Y. Yu, *RSC Adv.* **4**, 16920 (2014)
19. X.-Q. Zhang, Q. Sun, W. Dong, D. Li, A.-H. Lu, J.-Q. Mu, W.-C. Li, *J. Mater. Chem. A* **1**, 9449 (2013)
20. G. Wang, C. Pan, L. Wang, Q. Dong, C. Yu, Z. Zhao, J. Qiu, *Electrochim. Acta* **69**, 65 (2012)
21. E.J. Ra, E. Raymundo-Piñero, Y.H. Lee, F. Béguin, *Carbon* **47**, 2984 (2009)
22. C. Ma, Y. Song, J. Shi, D. Zhang, X. Zhai, M. Zhong, Q. Guo, L. Liu, *Carbon* **51**, 290 (2013)
23. J. Li, X. Wang, Y. Wang, Q. Huang, C. Dai, S. Gamboa, P.J. Sebastian, *J. Non-Cryst. Solids* **354**, 19 (2008)
24. F. Caturla, M. Molina-Sabio, F. Rodríguez-Reinoso, *Carbon* **29**, 999 (1991)
25. C. Ma, Y. Li, J. Shi, Y. Song, L. Liu, *Chem. Eng. J.* **249**, 216 (2014)
26. X. Liu, M. Antonietti, *Adv. Mater.* **25**, 6284 (2013)
27. H. Yin, L. Beihu, X. Yin, D. Tang, X. Mao, W. Xiao, D. Wang, A.N. Alshawabkeh, *Environ. Sci. Technol.* **48**, 8101 (2014)
28. X. Deng, B. Zhao, L. Zhu, Z. Shao, *Carbon* **93**, 48 (2015)

29. J. Wang, B. Ding, X. Hao, Y. Xu, Y. Wang, L. Shen, H. Dou, X. Zhang, *Carbon* **102**, 255 (2016)
30. C. Ma, Y. Song, J. Shi, D. Zhang, M. Zhong, Q. Guo, L. Liu, *Mater. Lett.* **76**, 211 (2012)
31. V.A. Davydov, A.V. Rakhmanina, V. Agafonov, B. Narymbetov, J.P. Boudou, H. Szwarc, *Carbon* **42**, 261 (2004)
32. B.-H. Kim, K.S. Yang, D.J. Yang, *Electrochim. Acta* **109**, 859 (2013)
33. S.-H. Yoon, S. Lim, Y. Song, Y. Ota, W. Qiao, A. Tanaka, I. Mochida, *Carbon* **42**, 1723 (2004)
34. W. Qiao, S.-H. Yoon, I. Mochida, *Energ. Fuel* **20**, 1680 (2006)
35. A. Linares-Solano, in *Chemistry and Physics of Carbon. Series: Chemistry and Physics of Carbon*. ed. by L. Radovic (CRC Press, Boca Raton, 2007), pp. 1–62. ISBN: 978-1-4200-4298-6
36. M. Wu, P. Ai, M. Tan, B. Jiang, Y. Li, J. Zheng, W. Wu, Z. Li, Q. Zhang, X. He, *Chem. Eng. J.* **245**, 166 (2014)
37. S. Biniak, G. Szymański, J. Siedlewski, A. Świątkowski, *Carbon* **35**, 1799 (1997)
38. C. Kim, K.S. Yang, *Appl. Phys. Lett.* **83**, 1216 (2003)
39. B.H. Kim, N.N. Bui, K.S. Yang, M.E. dela Cruz, J.P. Ferraris, *Bull. Korean Chem. Soc.* **30**, 1967 (2009)
40. Z. Dong, S.J. Kennedy, Y. Wu, *J. Power Sources* **196**, 4886 (2011)
41. C. Lai, Z. Zhou, L. Zhang, X. Wang, Q. Zhou, Y. Zhao, Y. Wang, X.-F. Wu, Z. Zhu, H. Fong, *J. Power Sources* **247**, 134 (2014)
42. Z. Liu, D. Fu, F. Liu, G. Han, C. Liu, Y. Chang, Y. Xiao, M. Li, S. Li, *Carbon* **70**, 295 (2014)
43. Y.-H. Hsu, C.-C. Lai, C.-L. Ho, C.-T. Lo, *Electrochim. Acta* **127**, 369 (2014)
44. C.H. Kim, B.-H. Kim, *Electrochim. Acta* **117**, 26 (2014)